# OH plus HONO reaction: A theoretical study

**ARTICLE** *in* JOURNAL OF MOLECULAR STRUCTURE THEOCHEM · DECEMBER 2007

Impact Factor: 1.37 · DOI: 10.1016/j.theochem.2007.08.037



**5 AUTHORS**, INCLUDING:

Jilai Li
Jilin University
**66** PUBLICATIONS **285** CITATIONS
SEE PROFILE

Dan Mu
Jilin University
**166** PUBLICATIONS **1,135** CITATIONS
SEE PROFILE

ELSEVIER

Journal of Molecular Structure: THEOCHEM 847 (2007) 10–22

THEO CHEM

www.elsevier.com/locate/theochem

# OH + HONO reaction: A theoretical study

De-Quan Wang, Ji-Lai Li, Xu-Ri Huang *, Cai-Yun Geng, Chia-Chung Sun

*State Key Laboratory of Theoretical and Computational Chemistry, Institute of Theoretical Chemistry, Jilin University, Changchun 130023, People's Republic of China*

Received 19 June 2007; received in revised form 24 August 2007; accepted 24 August 2007
Available online 11 September 2007

**Abstract**

The reaction of OH radical with nitrous acid HONO is investigated by ab initio quantum chemistry methods. The doublet potential energy surfaces are calculated at the CCSD(T)/aug-cc-pVDZ//UMP2/6-311++G(d,p) levels. Various possible reaction pathways are considered. Among them, the most feasible pathway should be the OH radical attacking on the hydrogen of *cis*-HONO to form a 6-member-ring complex C2 barrierlessly, followed by the indirect hydrogen abstraction transition state TSabsC2-C6I to form a weakly bound complex C6, giving rise to the educts P1 $H_2O + NO_2$. Because all of the complexes, transition state, and products involved in the feasible pathway lie below the reactants, the title reaction is expected to be rapid, which in good agreement experiment. The present study may be helpful for probing the mechanisms of the HONO reactions and understanding the atmospheric chemistry.


*Keywords:* Reaction mechanism; Potential energy surface; OH radical; HONO

## 1. Introduction

Radical-molecule reactions play important roles in both combustion and interstellar processes [1]. Reactions with small or even zero barriers are of particular interest [2–6], especially in interstellar space where the temperature is low. Under these conditions, low-barrier reactions easily deplete molecules and yield new products. The reaction of hydroxyl radical with nitrous acid is very important to the chemistry of troposphere where HONO may be formed by lighting or chemical reactions in the polluted environment. Surprisingly, data on non-reactive uptake of nitrous acid on ice are scarce, given the importance of HONO for atmospheric and especially polar snow chemistry [7–10]. On the other hand, the reaction is also pivotal to our understanding of high-temperature combustion of nitrate esters, nitramines and energetic materials containing [H, N, O]-species [11]. It has been long known that nitrous acid is a key reactive intermediate during the course of chemical combustion reactions of energetic materials such as nitramines propellants [12–15]. On account of its relevancy in combustion and atmospheric chemistry, kinetic and mechanistic information on H, O, $NO_2$, $O_3$, HCl, F, HF, HNO and $NH_3$ initiated reaction with nitrous acid has been subject to numerous experimental and theoretical studies [16–21].

The most important chemical cleaning agent of the atmosphere is the hydroxyl radical, OH [22,23]. It determines the oxidizing power of the atmosphere, and thereby controls the removal of nearly all gaseous atmospheric pollutants [24,25]. The atmospheric supply of OH is limited, however, and could be overcome by consumption due to increasing pollution and climate change [26,27], with detrimental feedback effects. Recently Rohrer etc. reported that the concentration of OH is linear dependence on solar ultraviolet radiation [28].

Literaturely, there have been limited but conflicting kinetic data [29–38] for the OH + HONO reaction, which has been invariably assumed to occur by the abstraction reaction:

$$OH + HNO_2 \rightarrow H_2O + NO_2 \quad \Delta H = -41 \text{ kcal/mol}$$

* Corresponding author. Fax: +86 431 8894 5942.
*E-mail address:* wangdq3@gmail.com (X.-R. Huang).

0166-1280/$ - see front matter © 2007 Elsevier B.V. All rights reserved.
doi:10.1016/j.theochem.2007.08.037

In the temperature range of interest to atmospheric chemistry, Cox and co-workers reported the rate constant at ambient temperature to fall within the range of $(1–4)\times10^{-12}$ cm$^3$ mol$^{-1}$ s$^{-1}$ with small positive activation energy, 3.2 kJ/mol, and independent of pressure [30–34]. Recently, Burkholder et al. [35] determined the rate constant by LIF (laser-induced fluorescence) for OH detection and reported $k_1 = (2.8 \pm 1.3)\times10^{-12}$ exp [(+260 ± 140)/T] cm$^3$ mol$^{-1}$ s$^{-1}$ for the temperature range 298–373 K. The activation energy for the reaction was found to be −2.2 kJ/mol, clearly at odds with that of Jenkin and Cox mentioned above. Furthermore, another two conflicting rate constant expressions have been recommended: $k_1 = 3.76\times10^{-12}$ T$^{1.0}$ exp (−68/T) cm$^3$ mol$^{-1}$ s$^{-1}$ for 300–2500 K by Tsang and Herron [36] for high-temperature combustion modeling applications, $k_1 = 1.63\times10^{-12}$ exp (+260/T) cm$^3$ mol$^{-1}$ s$^{-1}$ at 290–380 K by Atkinson et al. [37] for atmospheric modeling applications. On the other hand, a theoretical study [11a] on the title reaction was carried out, and the equilibrium geometries and transition structures were calculated using density functional theory (DFT) method. As we know, different in geometry will lead to different reaction mechanisms and extreme care should be taken to choose an appropriate theoretical level for investigation of reactions involving radicals [39].

Thus, it is necessary to reexamine the title reaction with other theoretical method to provide theoretical knowledge accurate enough to be useful for further kinetic and thermodynamic study on radical reactions. Some conclusions that are made in this work may be helpful for further theoretical and experimental studies of this title reaction.

In the title reaction there are pre-reactive complexes.

Six pre-reactive complexes are successfully located on the doublet PESs. All the six structures with no imaginary frequencies (minima) were located at all levels of theory. As shown in Fig. 1, most of the addition and the H-abstraction reactions proceed via complexes in the title reaction. Another theoretical investigation of the isoelectronic system $C_2H_2 + O^-$ [40], shows that a collinear hydrogen-bonded complex $C_2H^-\cdots OH$ (productlike) exist on the PES, which is viewed as a direct precursor for the proton transfer. While in another isoelectronic system $C_2H_2 + OH$, there is no pre-reactive complex located on the H-abstraction path, but on the addition path [41]. On the other hand, all the ab initio calculations show that the approach of H/O atom of OH radical to HONO generates six different initial pre-reactive complexes, depending on the details of the approach geometry.

## 2. Computational methods

All the calculations were carried out on the SGI O3800 servers using the GAUSSIAN 98 and GAUSSIAN 03 program package [42]. Geometries of the reactants, products, intermediates and transition states (TSs) have been optimized with the unrestricted Møller–Plesset second-order perturbation UMP2 (FULL) [43] method using the 6-311G(d,p), and 6-311++G(d,p) basis sets. The presence of diffuse functions in the basis set allows for an appropriate representation of the dispersion forces that should play an important role in the stabilization of the weakly bound structures considered in this work [44]. Vibrational frequencies, also calculated at the same level of theory, have been used to characterize stationary points, zero-point energy (ZPE) corrections calculations. The number of imaginary frequencies for intermediates and transition states are 0 and 1, respectively. The ZPE and vibrational frequencies were scaled by a factor of 0.95 for anharmonicity correction [45]. To confirm that the transition states connect between designated intermediates, intrinsic reaction coordinate (IRC) [46] calculations were performed at the UMP2/6-311++G(d,p) level of theory.

For the purpose of obtaining more reliable energies of various structures, the coupled-cluster CCSD(T) method with Dunning's correlation-consistent augmented aug-cc-pVDZ basis set [47,48] was used. The UMP2/6-311++G(d,p) optimized geometries were used for the single-point coupled cluster calculations without reoptimization at the CCSD(T)/aug-cc-pVDZ.

The major problem in the application of unrestricted single determinant reference wave function is that of contamination with higher spin states. The severe spin contamination could lead to a deteriorated estimation of the barrier height [49,50]. We have examined the spin contamination before and after annihilation for the radical species and transition states involved in the OH + HONO reaction. For doublet systems, the expectation values of $\langle S^2\rangle$ after annihilation range from 0.75 to 0.80 (the exact value for a pure doublet is 0.75) except for one complex and six unimportant transition states on the potential energy surface (0.80–0.87). This suggests that the wave function is not severely contaminated by states of higher multiplicity [51,52].Therefore, we expect that the CCSD(T)//MP2 calculations reported in this work are, in this regard, reliable.

The thermodynamic functions ($\Delta H$ and $\Delta G$) are estimated within the ideal gas, rigid-rotor, and harmonic oscillator approximations. A temperature of 298.15 K and a pressure of 1 atm were assumed.

## 3. Results and discussion

For the present $H_2NO_3$ system, there are enantiomorphs. For convenient and clear discussion, we only present moieties of reaction channels that have enantiomorphic varieties and some important nantiomorphous structures. The structures of the reactants, complexes, intermediate isomers, transition states and products are depicted in Fig. 1. By means of the interrelation among the reactants, isomers, transition states, and products as well as the corresponding relative energies, the schematic profiles of the doublet potential energy surfaces are depicted as shown in Figs. 2, 3 and Fig. S3. The calculated

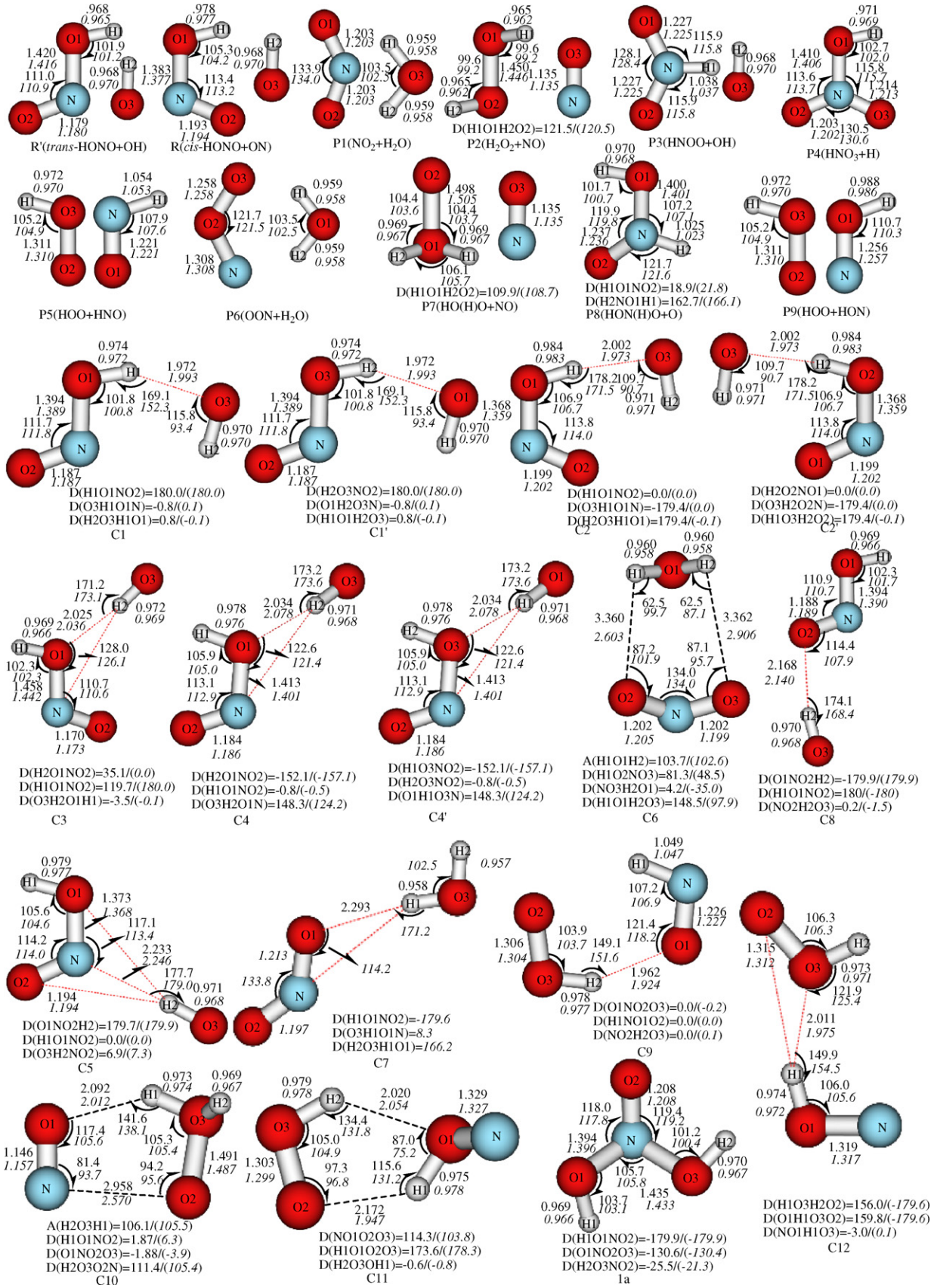


Fig. 1. Optimized geometries of the reactants, the complexes, the doublet intermediate isomers, the products and the transition states for the OH + HONO reaction. Bond distances are in angstroms, and angles are in degrees. Numbers in roman type show the structures at the UMP2/6-311++G(d,p) level of theory. Numbers in italics show the structures at the UMP2/6-311G(d,p) level of theory. Numbers in bold show the structures at the Max{CCSD(T)}//IRC{UMP2} + ZPE level of theory. Symbols with asterisks indicate enantiomorphic varieties corresponding to the same symbols.

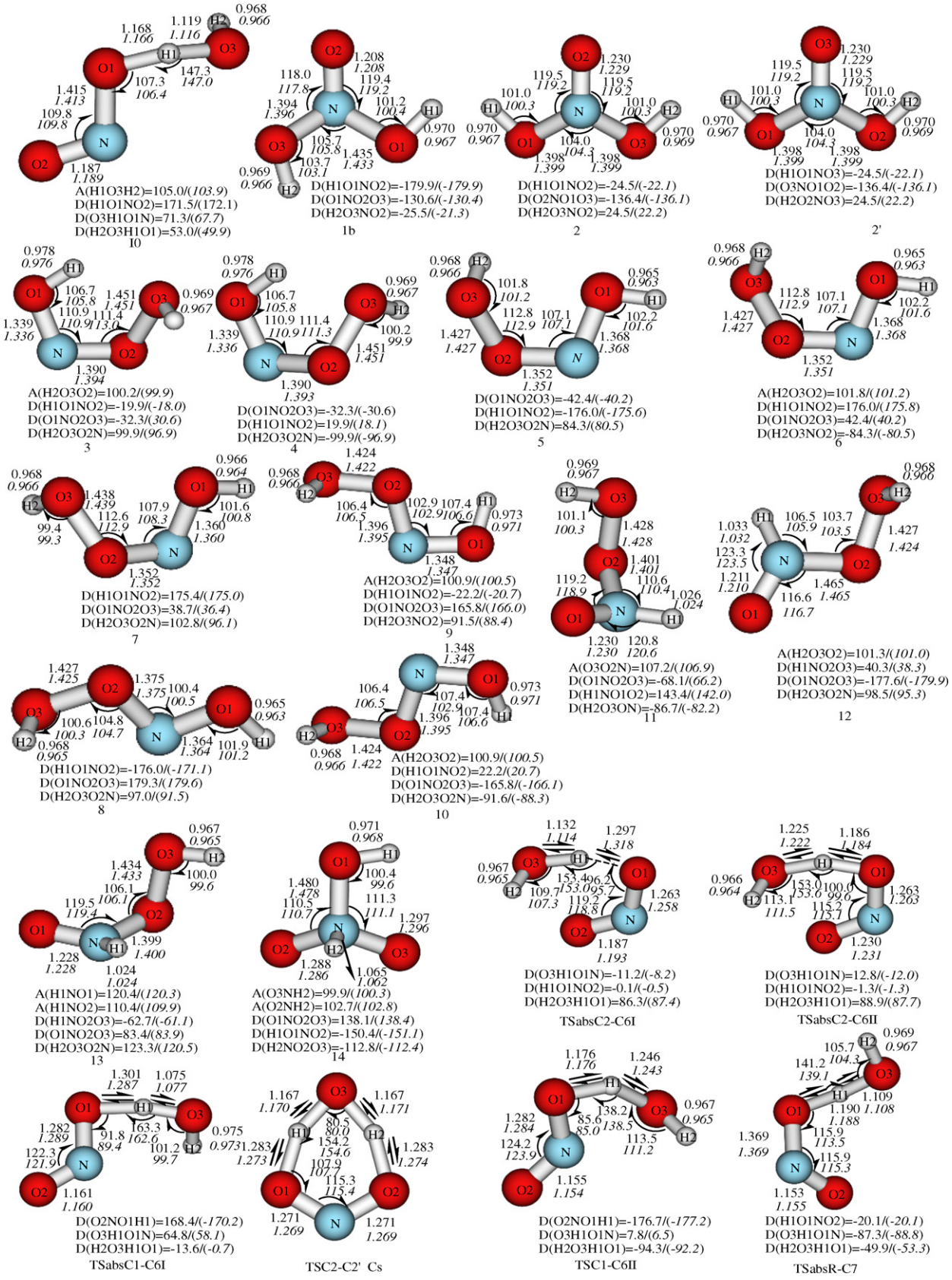


Fig. 1 (*continued*)

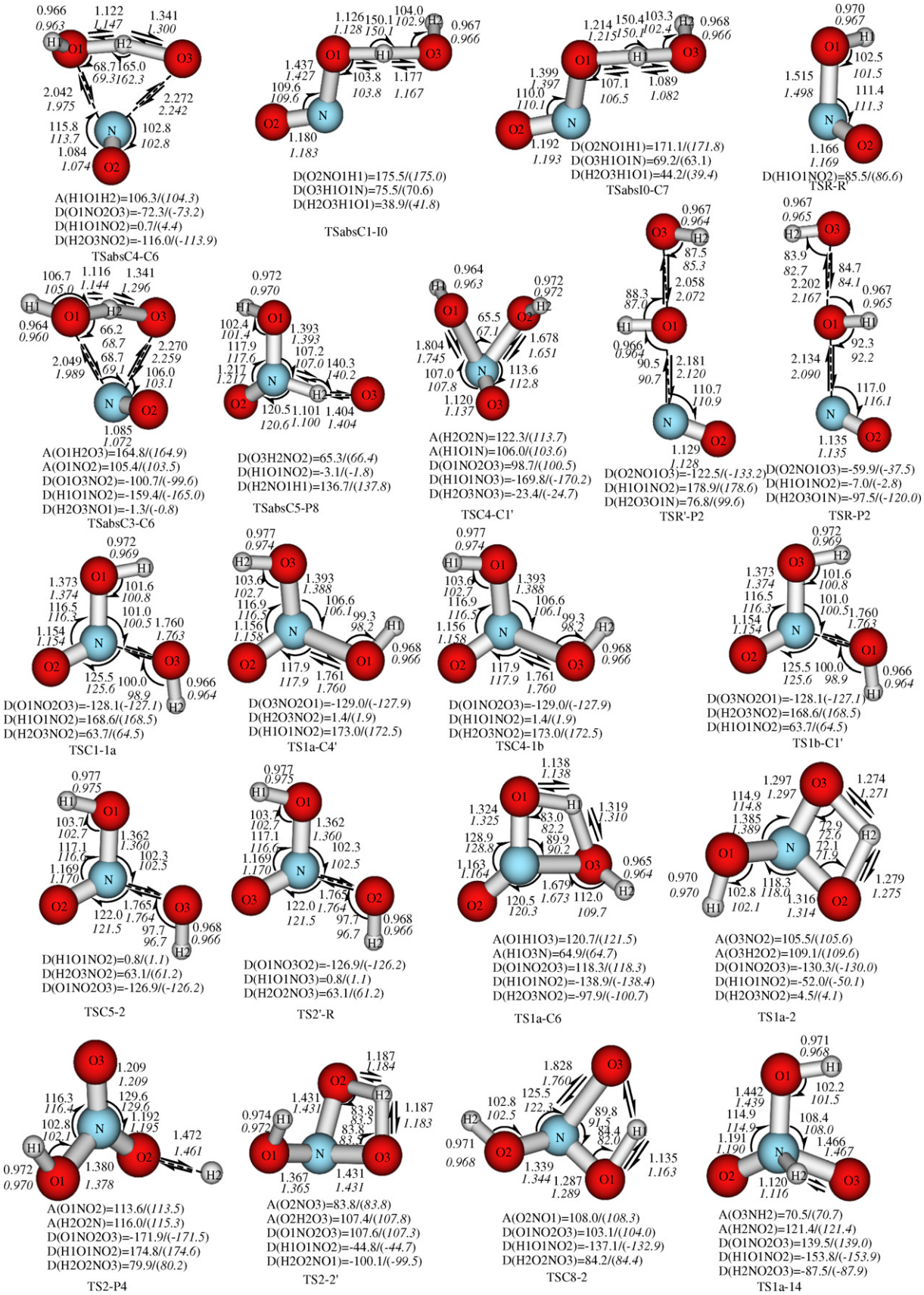


Fig. 1 (*continued*)

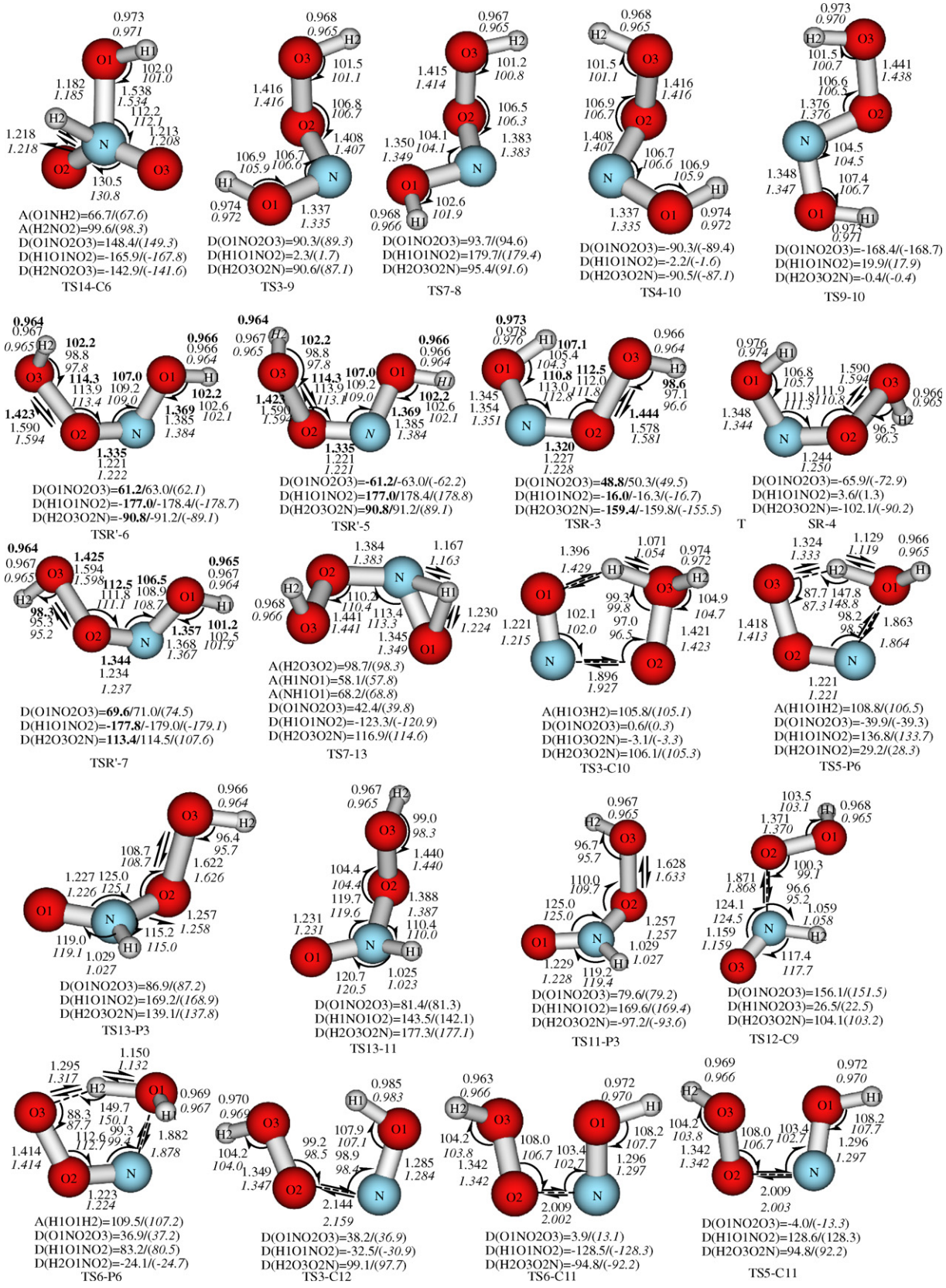


Fig. 1 (*continued*)

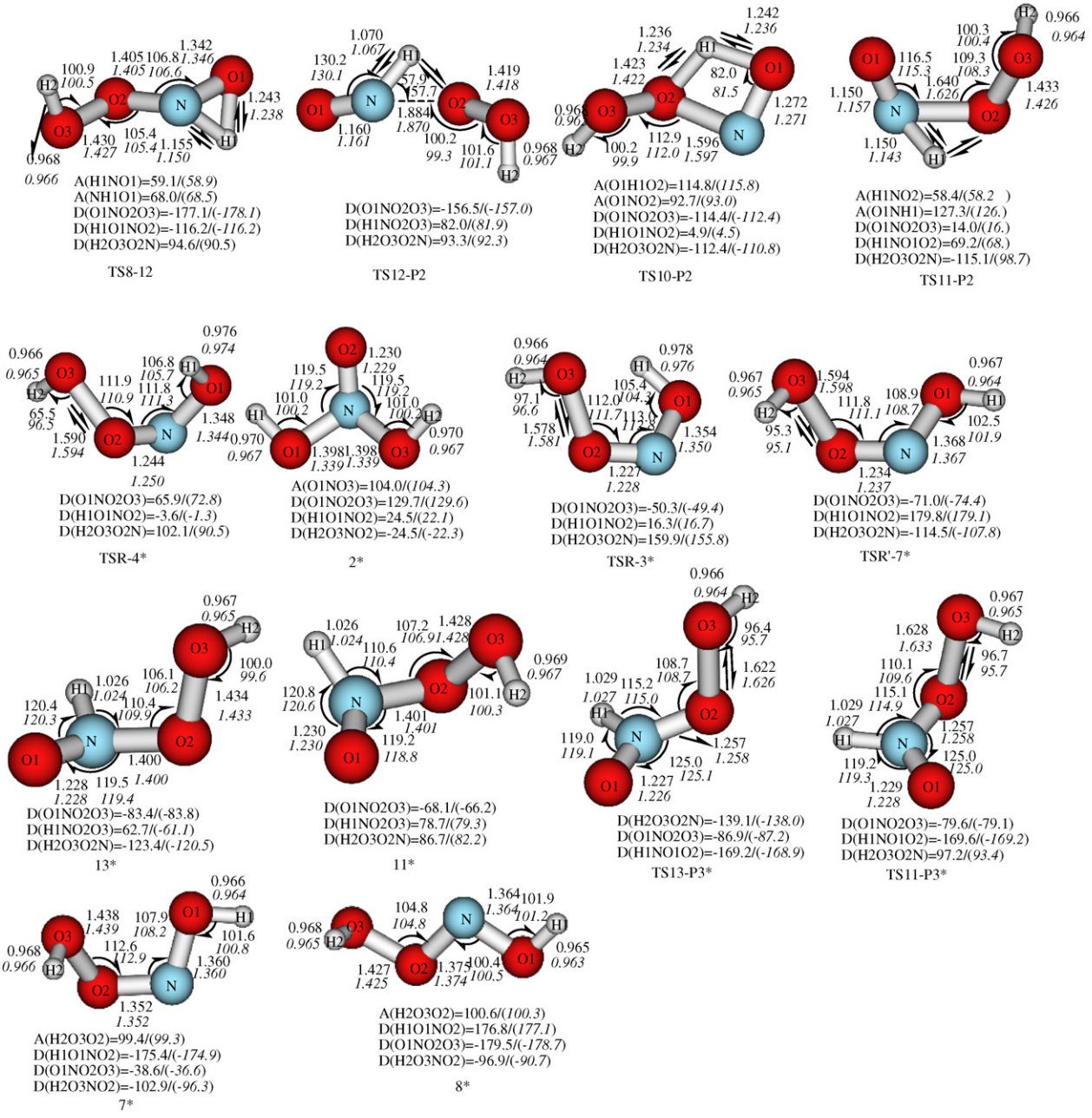


Fig. 1 (*continued*)

energetic data ($\Delta E$, $\Delta H$, and $\Delta G$) of various complexes, isomers, transition states and products are listed in Table S1. For convenient discussion, the energy of OH + *cis*-HONO is set at zero as a reference for other species.

### 3.1. Analysis of reaction mechanism of OH radical with HONO

As the OH + HONO reaction can have either an abstraction or an addition mechanism, three distinguishable types of initial attacks have been revealed for the radical-molecule reaction OH + HONO, namely, the picking-up on hydrogen (direct/indirect hydrogen abstraction), hydroxyl (direction hydroxyl abstraction), and the attack on the O-atom and N-atom of HONO (addition–isomerization–elimination). A detailed discussion on the title reaction mechanism is given as follows.

#### 3.1.1. Hydrogen abstraction reaction mechanism

Three kinds of hydrogen abstraction reactions can take place in the title reaction, viz. the oxygen of the OH radical picking-up hydrogen of HONO directly or indirectly (single-barrier and double-barriers), and the O/N-atom of the HONO indirect picking-up hydrogen of OH radical.

##### 3.1.1.1. The oxygen of OH radical attack on the hydrogen of HONO. Indirect hydrogen abstraction reaction mechanism I

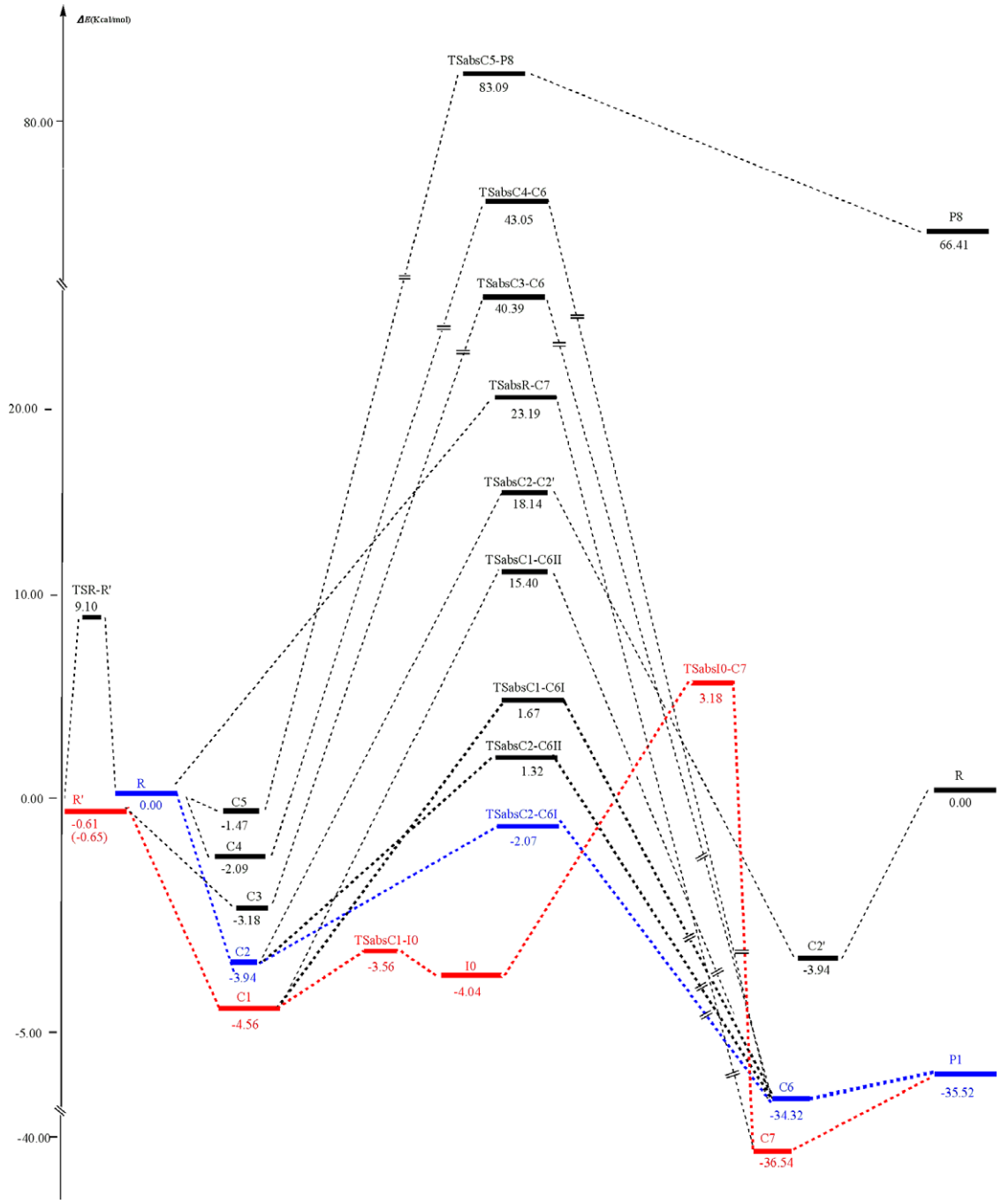


Fig. 2. Schematic potential energy surfaces of the hydrogen abstraction channels in the OH + HONO reaction. Numbers in roman type are relative energies at the CCSD(T)/aug-cc-pVDZ//UMP2/6-311++G(d,p) + ZPE level of theory. Relative energy of complex C7 is calculated at the CCSD(T)/aug-cc-pVDZ//UMP2/6-311G(d,p) + ZPE level of theory.

*(single-barrier hydrogen abstraction)*. The first step of this mechanism involves the O atom of OH radical indirectly attacking the H-atom of HONO. For *cis*-HONO, there are three pathways of the indirect hydrogen abstraction reactions, and for *trans*-HONO, two. These pathways can be expressed as follows:

Path1 RP1 (1): R (*cis*-HONO + OH) → C2 → T-SabsC2-C6I → C6 → P1 $NO_2 + H_2O$
Path2 RP1 (2): R → C2 → TSabsC2- C6II → C6 → P1
Path3 RR (1): R → C2 → TSabsC2- C2′ → C2′ → R
Path4 R′P1 (1): R′ (OH + *trans*-HONO) → C1 → T-SabsC1- C6I → C6 → P1
Path5 R′P1 (2): R′ → C1 → TSabsC1- C6II → C6 → P1

As shown in Fig. 2, the first two indirect hydrogen abstraction processes start from the OH radical attacking on the hydrogen of *cis*-HONO, forming a 6-member-ring complex C2 (−3.94 kcal/mol) barrierlessly. And then C2 can transform to a weakly bound complex C6 (−34.32)

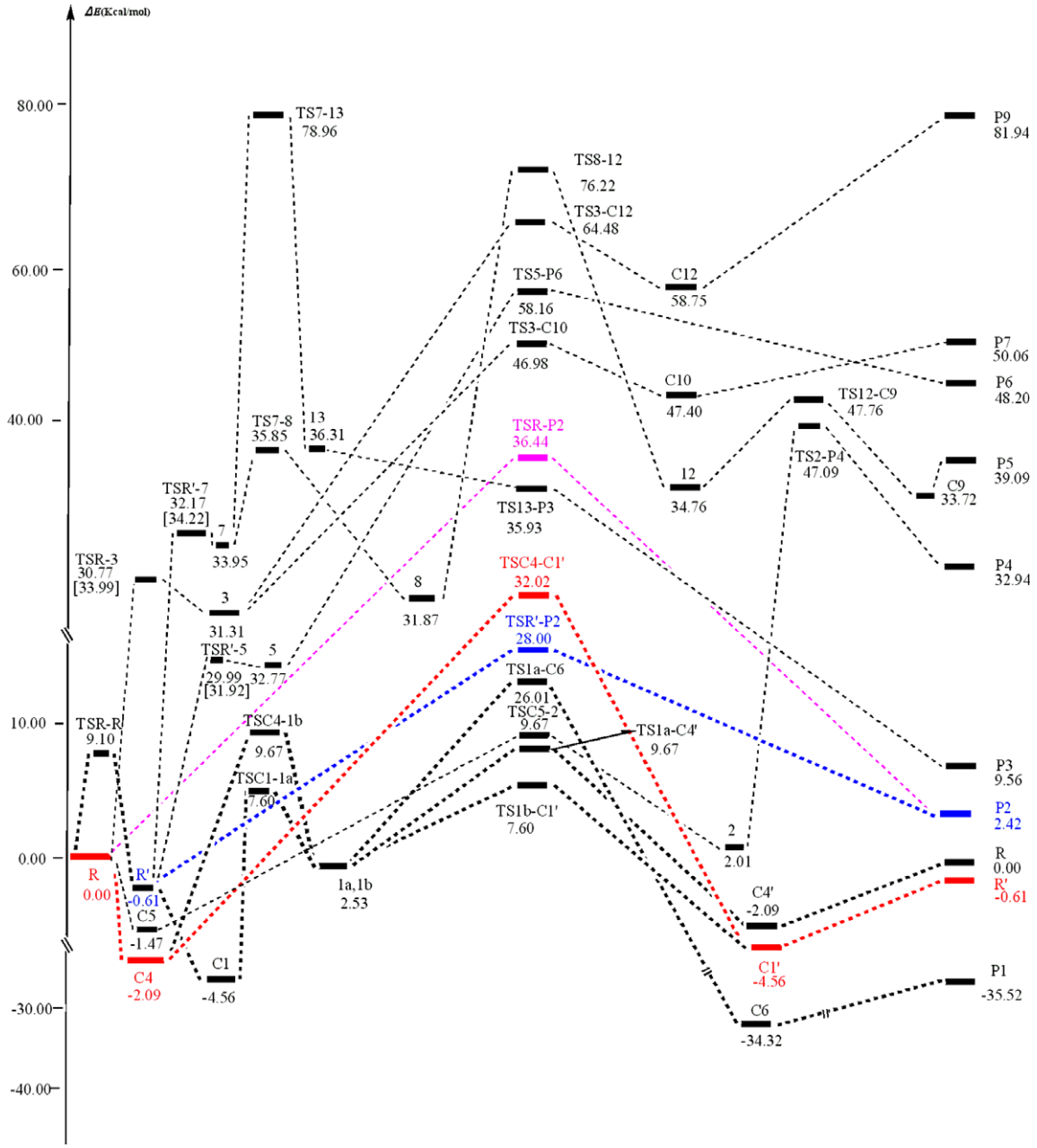


Fig. 3. Selected schematic potential energy surfaces of the associative reaction mechanism, and the important addition–isomerization–elimination channels in the OH + HONO reaction. Numbers in roman type are relative energies at the CCSD(T)/aug-cc-pVDZ//UMP2/6-311++G(d,p) + ZPE level of theory. Numbers in square brackets are values at the Max-{CCSD(T)}//IRC{UMP2} + ZPE level of theory.

via two H-atom abstraction transition states, TSabsC2-C6I (−2.07) and TSabsC2-C6II (1.32), respectively. Subsequently, C6 transforms to the educts P1 $H_2O + NO_2$. Since all of the complexes, transition state and products lie below the reactants, the rate of this pathway should be very fast even in low-temperature ranges. On the other hand, considering that the rate-determining transition state TSabsC2-C6II lies 1.32 kcal/mol above the reactants in Path2, we can safely draw the conclusion that the reaction pathway Path2 is also feasible on the doublet potential energy surface at room-temperature. However, the higher rate-determining energy barrier in Path2 makes Path2 less competitive than Path1.

Pathway Path3 is indeed an H-atom exchange process between OH radical and *cis*-HONO. In pathway Path3, complex C2 and C2′ can be formed barrierless with the association of hydroxyl and *cis*-HONO. Complex C2 (C2′) can transform to C2′ (C2) via TSabsC2-C2′, with an 18.14 kcal/mol energy barrier. Both complexes, C2 and C2′ located by IRC calculations, are essentially the mirror image of each other, having −3.94 kcal/mol binding energies with $C_s$ symmetry. Furthermore, a similar exchange process involving the *trans*-HONO does not exist.

The OH radical and *trans*-HONO can also form a 5-member-ring complex C1 in pathways Path4 and Path5.

Complex C1 has a slightly larger binding energy (−4.56) than its *cis*-counterpart C2. For products formation, however, C1 has to overcome energy barriers TSabsC1-C6I (1.67 kcal/mol), or TSabsC1-C6II (15.40 kcal/mol) to reach C6, in Path4 and Path5, respectively. Thus the indirect hydrogen abstraction process of *trans*-HONO by OH may proceed through Path4.

*Indirect hydrogen abstraction reaction mechanism II (double-barriers hydrogen abstraction).* There exists a remarkable difference between the *trans* and *cis* reaction processes, that is, for the OH radical picking-up the H-atom of *trans*-HONO process, there is a double-barriers hydrogen abstraction reaction mechanism, viz. indirect hydrogen abstraction reaction mechanism II. To our knowledge, it is the first time that the existence of double barriers in hydrogen abstraction reactions has been reported. The pathway Path7 takes place via the complex C1, transition state TSabsC1-I0, isomer I0, transition state TSabsI0-C7 and the complex C7, giving rise to the separated $H_2O + NO_2$ products with the energies of −4.56, −3.56, −4.04, 3.18 and −34.54 kcal/mol, respectively. As shown in Fig. 2, the rate-determining transition state TSabsI0-C7 in Path6 lies somewhat higher than that of Path1, Path2 and Path4, which leads us to the fact that the Path6 is less competitive than those three pathways, but it could also occur at room-temperature. It can be expressed as follows:

Path6 R′P1 (3): R′ → C1 → TSabsC1- I0 → I0 → TSabsI0-C7 → C7 → P1

*Direct hydrogen abstraction reaction mechanism.* Among all the OH radical attack on the H-atom of HONO pathways, only one direct hydrogen abstraction reaction path is revealed in the present investigation. We express it below for discussion concision:

Path7 RP1 (3): R → TSabsR-C7 → C7 → P1

In this pathway, the rate-determining hydrogen abstract transition state TSabsR-C7 lies 23.19 kcal/mol higher than the reactants, the rate of this pathway should be very slow at moderate conditions. Consequently, the large barrier also prevents it from competing effectively with the reaction pathways Path1 and Path2. We should mention herein that we could not find the complex C7 at the UMP2/6-311++G(d,p) level. To rationalize this situation, we turn to the flatness of the PES in the regions of larger intermolecular distances as can be seen from Fig. 1.

To briefly summarize, the pathway Path1 is the most competitive pathway among all of the seven pathways. The pathway Path2, Path4 and path6 may be less competitive dynamically and play a part role at room temperature.

*3.1.1.2. The hydrogen of OH radical attack on the O/N-atom of HONO.* Our results show that there are additional three hydrogen abstraction reaction channels, namely, the hydrogen of OH radical attacking on hydroxyl-oxygen, and nitrogen-atom of HONO. They are listed as follows:

Path8 RP1 (4): R → C4 → TSabsC4-C6 → C6 → P1
Path9 R′P1 (5): R′ → C3 → TSabsC3-C6 → C6 → P1
Path10 RP8 (4): R → C5 → TSabsC5-P8 → P8 HON(H)O + O

As shown in Fig. 1, transition states TSabsC4-C6 (43.05) and TSabsC3-C6 (40.39) possess similar 4-member-ring structures in Path8 and Path9. In these two reaction pathways, IRC calculations show that, the hydrogen of OH radical approaches the hydroxyl-oxygen of HONO firstly, which makes the bond of HO···NO broken, and then, the O···H bond of OH radical ruptured. Secondly, the O-atom attacks the N-atom of NO, forming the complex C6, leading to P1 eventually. On the other hand, the hydrogen of OH radical can also attack on the nitrogen of *cis*-HONO, leading to the production of P8 HON(H)O + O through Path10. Since the rate-determining energy barrier in Path10 is considerably high (83.09), we can safely rule it out from the doublet PES in low-temperature ranges. However, in combustion environment, where the temperature is very high (>1000 K), pathways Path8 and Path9, may play an important role.

*3.1.2. Associative reaction mechanism*

There are three reaction channels in the associative reaction mechanism, that is, Path11 ∼ 13, in which three associative transition structures are successfully established. The paths are listed below:

Path11 R′P2 (1): R′ → TSR′-P2 → P2 $H_2O_2$ + NO
Path12 RP2 (1): R → TSR-P2 → P2
Path13 RR′ (3): R → C4 → TSC4-C1′ → C1′ → R′

As shown in Fig. 1, the main feature of the transition state TSR′-P2 in the path11 is: It has an imaginary frequency of 228i $cm^{-1}$ and the animation of imaginary frequency corresponds to the movement of OH and NO group, when OH moves toward the O-atom of hydroxyl in *trans*-HONO, the NO group would be away from it, that is to say, the formation of the O–O bond is concomitant with the breaking of the O–N bond. A corollary, the formation of the O–N bond would be concomitant with the breaking of the O–O bond. The transition states TSR-P2 and TSC4-C1′ own the similar feature as well except the different moving groups. That is, TSR-P2 corresponds to the movement of OH radical and NO in *cis*-HONO, which is reported for the first time, while TSC4-C1′ corresponds to the movement of the OH radical and OH in *cis* or *trans*-HONO.

As shown in Fig. 3, there are six pathways can lead to products P2 $H_2O_2$ + NO. In the six pathways, the most two possible pathways are the Path11 and Path12 mentioned above. One can find that, the rate-determining energy barriers, TSR′- P2 (28.00) and TSR-P2 (36.44), are higher than those in the hydrogen abstraction path-

ways, and consequently, products P2 should be the minor product compared with P1 in the title reaction for kinetics and thermodynamics points of view in all temperature ranges.

*3.1.3. Addition–isomerization–elimination mechanism*

As shown in Fig. 3, the rest reaction channels belong to addition–isomerization–elimination mechanism, which is more complex than previous report [11a]. For discussion concision, we just focus our attention on the minimum energy pathways (MEP) of products P1, P3 ~ 7, P9 and *cis–trans* isomerization reactions.

*3.1.3.1. P1 $NO_2 + H_2O$ formation.* There are other four pathways can lead to products P1. The most feasible pathway is an addition–H-shift–elimination reaction process. It is listed below:

Path14 R′P1 (6): R′ → C1 → TSC1-1a → 1a → TS1a- C6 → C6 → P1

*3.1.3.2. P3 ~ 7, P9 formation.* In these reaction steps the high relative energy of rate-determining transition states may rule out their significance in atmospheric chemistry in low temperatures, and even in higher temperature ranges. For conciseness, we only list them as follows:

Path15 R′P3 (1): R′ → TSR′-7 → 7 → TS7- 13 → 13 → TS13-P3 → P3 HNOO + OH
Path16 RP4 (1): R → C5 → TSC5- 2 → 2 → TS2-P4 → P4. $HNO_3$ + H
Path17 R′P5 (1): R′ → TSR′-7 → 7 → TS7- 8 → 8 → TS8-12 → 12 → TS12-C9 → C9 → P5 HOO + HNO
Path18 R′P6 (1): R′ → TSR′-5 → 5 → TS5- P6 → P6 OON + $H_2O$
Path19 RP7 (1): R → TSR-3 → 3 → TS3-C10 → C10 → P7 HO(H)O + NO
Path20 RP9 (1): R → TSR-3 → 3 → TS3-C12 → C12 → P9 HOO + HON

We should mention that, as shown in Fig. 3, four isomers 3 (31.31), 5 (32.77), and 7 (33.95) formation processes are in low potential well at the CCSD(T)//aug-cc-pVDZ level of theory. This implies that such isomers might be short-lived and not important on the PES [53] and can be safely ruled out. On the other hand, one can find that the oxygen of OH radical attack on terminal O-atom of HONO mechanisms processes involve negative barriers at CCSD(T)//aug-cc-pVDZ levels. In contrast, the IRCMax method consistently gives positive barriers that differ from the CCSD(T)//aug-cc-pVDZ levels by 2–3 kcal/mol with sizable displacements along the reaction path ($0.7 < S < 1.0$,). We expect that large errors are due to poor transition state geometries and positions along the IRCs at a low level of theory and thus have considerable effects on the calculated energy barriers.

*3.1.3.3. The OH radical exchange reactions.* There are other two reaction pathways for the OH radical exchanges with the OH group in HONO except for Path13 which is mentioned in the section 3.1.2. One can find, from Fig. 3, that both the barriers involved in the OH exchange pathways are moderate ($\Delta E$<10; $\Delta G$ < 18 kcal/mol) and the exchange processes are not endothermic. Therefore, both kinetic and thermodynamic considerations support the viability of such channels. We simply list them below for concision:

Path21 RR′ (1): R → C4 → TSC4- 1b → 1b → TS1b-C1′ → C1′ → R′
Path22 R′R (1): R′ → C1 → TSC1- 1a → 1a → TS1a-C4′ → C4′ → R

*3.2. Comparison with experiments*

Recently, Robert A. Fifer [29] carried out the kinetic study for the title reaction. The reaction heats of formation calculated are in good agreement with that obtained experimentally. In the experiment, they suggested that the $NO_2 + H_2O$ formation is the most important channel for this chemical reaction. On the other hand, the speculated that *cis*-HONO is chiefly responsible for the abstraction reaction. However, they did not provide unambiguous information on the H-atom abstraction channel. Furthermore, they did not give any information about the formation of $H_2O_2 + NO$, which may be found in high temperature ranges.

In our calculations, it is shown that the most feasible pathway Path1 is the OH radical indirectly abstracts the H-atom of *cis*-HONO leading to the products P1 $NO_2 + H_2O$. Since the energies of the complexes, transition state and products in this pathway are lower than that of the reactants, the rate of this pathway should be very fast and have negative temperature dependence. This is qualitatively consistent with the experimental results [29,35]. The other three pathways Path2, Path4 and Path6 may play a part role at room temperature. Finally, it should be pointed out that in our calculations that the products $H_2O_2 + NO$ might be found in the title reaction system in high temperature conditions.

*3.3. Comparison with previous theory study*

The title reaction has been reported by Xia etc. [11a]. Geometry optimization and vibrational frequency calculations were carried out at the density functional B3LYP method with the 6-311G(*d*) basis set. There are some differences between the two studies, the details as show below.

In our studies we find that the hydrogen abstraction reaction mechanism is more complex than previous thought. The reaction mechanisms involved are: Single-barrier indirect hydrogen abstraction reaction mechanism, double-barriers indirect hydrogen abstraction reaction mechanism, and direct hydrogen abstraction reaction

mechanism. We present twelve reaction pathways through which the reaction can lead to products P1 $NO_2 + H_2O$, including the pathways that the hydrogen of the OH radical attack on hydroxyl-oxygen of HONO, which have not been reported previously. Furthermore, we also find the pathway of the hydrogen of the OH attack on nitrogen of HONO and the pathway of the hydrogen of the OH radical attack on the terminal oxygen at the same time the oxygen of the OH radical attack on nitrogen of HONO. In addition, several more complex pathways are also revealed, namely, the oxygen of OH radical attack on the terminal oxygen of HONO. Considering that the activation barriers and/or the relative energies of products are high, the title reaction may proceed under combustion environment, where the temperature is very high (>1000 K), and these pathways may play a part role and should be helpful for the reverse reactions.

### 3.4. Comparison with the reactions of H + HONO and F + HONO

To deepen understand the reaction mechanism of OH + HONO, it is worthwhile to compare the title reaction with analogous reaction H + HONO, and F + HONO which have been studied theoretically [16,18]. Theoretical calculations show that they exist in similarity and discrepancy. The similarity of the three reactions is that the *cis*-HONO isomer is apparently more reactive, as has been concluded in the $NH_2$ + HONO reaction [54]. On the other hand, the discrepancy lies in the competition abilities of pathways. For H + HONO reaction, the direct H-abstraction reactions is a minor process and that the indirect metathetical reactions taking place by H-atom addition to the N-atom as well as to the terminal O-atom, producing HNO + OH and NO + $H_2O$, are the dominant reaction channels. For the reaction of F + HONO, the most feasible reaction pathway is the direct H-abstraction reaction lead to $NO_2$ + HF. For OH + HONO, the most feasible reaction pathways are the indirect H-abstraction reactions leading to P1 $NO_2 + H_2O$, which is analogous with the reaction F + HONO. The other feasible pathways are the oxygen of the OH radical attack on nitrogen of HONO proceeding the direct hydroxyl exchange and the oxygen of the OH radical attack on hydroxyl-oxygen of HONO transforming to educts P2 $H_2O_2$ + NO. It is obvious that the reaction of OH + HONO involves all the main features of H + HONO and F + HONO reactions. However, from the discussions above, it is obvious that the reaction mechanisms of OH + HONO are more complicated than those of H + HONO and F + HONO.

## 4. Conclusions

A detailed theoretical survey on the complicated doublet PESs of the reaction of OH radical with nitrous acid HONO has been performed at the CCSD(T)//UMP2 levels of theory. Three different mechanisms and four major pathways are revealed in the present study. In the hydrogen abstraction reaction mechanism, the major pathways are Path1, Path2, Path4 and Path6 on the doublet PES. The pathway Path1 is the most competitive while pathway Path6 is least competitive among the four major pathways. In Path1, the indirect hydrogen abstraction process starts from the OH radical attacking on the hydrogen of *cis*-HONO, forming a 6-member-ring complex C2 with no energy barrier. And then C2 can transform to a weakly bound complex C6 via an H-atom abstraction transition state TSabsC2-C6I. Subsequently, C6 transforms to the separated products P1 $H_2O + NO_2$ directly. Since the relative energies of the complexes, transition state and products in this pathway lie lower than that of the reactants, the rate of this pathway should be very fast and have negative temperature dependence. On the other hand, our calculation results show that, in terms of potential energy surface, the title reaction involves all the main features of H + HONO and F + HONO reactions. However, the mechanisms of OH radical with HONO are rather more complicated than those two reactions. According to our results, the presence of prereactive complexes indicates that the simple hydrogen abstraction in the radical reaction with carbon-free compounds should be more complex. Based on the analysis of the energetics of all channels through which the abstraction, association, and addition reactions proceed, we expect that the reaction varieties should be considerable complicated for the title reaction under different experimental conditions. Therefore, future experimental studies on the title reaction are highly desirable under various pressures and temperatures. All in all, the present work will provide useful information for understanding the processes of OH radical reactions with other carbon-free compounds.

## Acknowledgements

This work is supported by the National Natural Science Foundation of China (Nos. 20073014, 20643004 and 20103003), Excellent Young Teacher Foundation of the Ministry of Education of China, Excellent Young Foundation of Jilin Province and Technology Development Project of Jilin Province (No. 20050906-6).

## Appendix A. Supplementary data

Table S1 gives the energies, enthalpies, and Gibbs free energies. Table S2 shows the values of the spin contamination before and after annihilation. Fig. S1 gives schematic potential energy surfaces of the associative reaction mechanism, and the addition-isomerization-elimination channels. This material is available free of charge via the Internet at E-mail: wangdq3@gmail.com. Supplementary data associated with this article can be found, in the online version, at doi:10.1016/j.theochem.2007.08.037.

## References


[1] W.A. San, M.C. Lin, in: Z. Afassi (Ed.), Chemical Kinetics of Small Organic Radicals, vol. III, CRC Press, Boca Raton, FL, 1988.
[2] Z.X. Wang, M.B. Huang, R.Z. Liu, Can. J. Chem. 75 (1997) 996.
[3] J.E. Butler, J.W. Fleming, M.C. Lin, Chem. Phys. 35 (1981) 355.
[4] M.R. Berman, M.C. Lin, Chem. Phys. 82 (1983) 435.
[5] A. Faure, C. Rist, P. Valiron, Chem. Phys. 241 (1999) 29.
[6] S.A. Carl, R.M.I. Elsamra, R.M. Kulkarni, H.M.T. Nguyen, J. Peeters, J. Phys. Chem. A 108 (2004) 3695.
[7] H. Thomas, A. Markus, P. Thomas, Chem. Rev. 106 (2006) 1375.
[8] J.Y. Park, Y.W. Lee, J. Phys. Chem. 92 (1988) 6294.
[9] L. Chu, G.W. Diao, L.T. Chu, J. Phys. Chem. A 104 (2000) 3150.
[10] F.F. Fenter, M.J. Rossi, J. Phys. Chem. 100 (1996) 13765.
[11] (a) W.S. Xia, M.C. Lin, Phys. Chem. Comm. 13 (2000) 1;
(b) E.W.G. Diau, M.C. Lin, Y. He, C.F. Melius, Prog. Energy Combust. Sci. 21 (1995) 1;
(c) D. Chakraborty, M.C. Lin, Prog. Astronaut. Aeronaut. 185 (2000) 33.
[12] K.K. Kuo, M. Summerfield, Fundamentals of solid propellant combustionProgress in Astronautics and Aeronautics, vol. 90, AIAA, Inc., New York, 1984.
[13] M.H. Alexander, P.J. Dagdigian, M.E. Jacox, C.E. Kolb, C.F. Melius, Prog. Energu. Combust. Sci. 17 (1991) 263.
[14] G.F. Adams, R.W. Shaw Jr., Annu. Rev. Phys. Chem. 43 (1992) 11.
[15] A.M. Mebel, M.C. Lin, K. Morokuma, C.F. Melius, J. Phys. Chem. 99 (1995) 6842.
[16] C.Y. Geng, J.L. Li, X.R. Huang, C.C. Sun, Chem. Phys. 324 (2006) 474.
[17] X. Lu, J. Park, M.C. Lin, J. Phys. Chem. A 104 (2000) 8730.
[18] C.C. Hsu, M.C. Lin, A.M. Mebel, C.F. Melius, J. Phys. Chem. A 101 (1997) 60.
[19] X. Lu, R.N. Musin, M.C. Lin, J. Phys. Chem. A 104 (2000) 5141.
[20] E.W. Kaiser, S.M. Japar, J. Phys. Chem. 82 (1978) 2753.
[21] Z. Latajka, Z. Mielke, A. Olbert-Majkut, R. Wieczorek, KG. Tokhadze, Phys. Chem. Chem. Phys. 1 (1999) 2441.
[22] H. Levy, Science 173 (1971) 141.
[23] D.H. Ehhalt, Science 279 (1998) 1002.
[24] D.J. Jacob, in: T.D. Potter, B.R. Colman (Eds.), Handbook of Weather, Climate and Water, 29, 2003, Springer, Berlin.
[25] J. Lelieveld, F. J Dentener, W. Peters, M.C. Krol, Atmos. Chem. Phys. 4 (2004) 2337.
[26] R.G. Prinn, J. Huang, R.F. Weiss, D.M. Cunnold, P.J. Fraser, P.G. Simmonds, A. McCulloch, C. Harth, P. Salameh, S. O'Doherty, R.H.J. Wang, L. Porter, B.R. Miller II, Science 292 (2001) 1882.
[27] M.R. Manning, D.C. Lowe, R.C. Moss, G.E. Bodeker, W. Allan, Nature 436 (2005) 1001.
[28] F. Rohrer, H. Berresheim, Nature 442 (2006) 184.
[29] R.A. Fifer, J. Phys. Chem. 80 (1976) 27.
[30] R.A. Cox, J. Photochem. 3 (1974) 291.
[31] R.A. Cox, J. Photochem. 3 (1974) 175.
[32] R.A. Cox, R.G. Derwent, P.M. Holt, J. Chem. Soc. Faraday Trans. 1 72 (1976) 2031.
[33] R.A. Cox, R.G. Derwent, P.M. Holt, J.A. Kerr, J. Chem. Soc. Faraday Trans. 1 72 (1976) 2044.
[34] M.E. Jenkin, R.A. Cox, Chem. Phys. Lett. 137 (1987) 548.
[35] J.B. Burkholder, A. Mellouki, R. Talukdar, A.R. Ravishankara, Int. J. Chem. Kinet. 24 (1992) 711.
[36] W. Tsang, J.T. Herron, J. Phys. Chem. Ref. Data. 20 (1991) 609.
[37] (a) R. Atkinson, D.L. Baulch, R.A. Cox, R.F. Hampson Jr., J.A. Kerr, J. Troe, J. Phys. Chem. Ref. Data 18 (1989) 88;
(b) R. Atkinson, D.L. Baulch, R.A. Cox, R.F. Hampson Jr., J.A. Kerr, J. Troe, J. Phys. Chem. Ref. Data 21 (1992) 1125.
[38] W.B. DeMore, S.P. Sander, D.M. Golden, R.F. Hampson, M.J. Kurylo, C.J. Howard, A.R. Ravishankara, C.E. Kolb, M.J. Molina, JPL Publication, Jet Propulsion Laboratory, Pasadena, CA, 1997, p. 97.
[39] P. Branã, B. Mene'ndez, T. Ferna'ndez, J.A. Sordo, J. Phys. Chem. A 104 (2000) 10842.
[40] L. Liu, Y. Li, J.M. Farrar, J. Chem. Phys. 123 (2005) 094304.
[41] J.B. Davey, M.E. Greenslade, M.D. Marshall, M.I. Lester, M.D. Wheeler, J. Chem. Phys. 121 (2004) 3009.
[42] (a) M.J. Frisch, G.W. Trucks, H.B. Schlegel, G.E. Scuseria, M.A. Robb, J.R. Cheeseman, V.G. Zakrzewski, J.A. Montgomery Jr., R.E. Stratmann, J.C. Burant, S. Dapprich, J.M. Millam, A.D. Daniels, K.N. Kudin, M.C. Strain, O. Farkas, J. Tomasi, V. Barone, M. Cossi, R. Cammi, B. Mennucci, C. Pomelli, C. Adamo, S. Clifford, J. Ochterski, G.A. Petersson, P.Y. Ayala, Q. Cui, K. Morokuma, D.K. Malick, A.D. Rabuck, K. Raghavachari, J.B. Foresman, J. Cioslowski, J.V. Ortiz, B.B. Stefanov, G. Liu, A. Liashenko, P. Piskorz, I. Komaromi, R. Gomperts, R.L. Martin, D.J. Fox, T. Keith, M.A. AlLaham, C.Y. Peng, A. Nanayakkara, C. Gonzalez, M. Challacombe, P.M.W. Gill, B.G. Johnson, W. Chen, M.W. Wong, J.L. Andres, M. Head-Gordon, E.S. Replogle, J.A. Pople, Gaussian 98, revision A.11; Gaussian, Inc.: Pittsburgh, PA, 1998.;
(b) M.J. Frisch, G.W. Trucks, H.B. Schlegel, G.E. Scuseria, M.A. Robb, J.R. Cheeseman, J.A. Montgomery Jr., T. Vreven, K.N. Kudin, J.C. Burant, J.M. Millam, S.S. Iyengar, J. Tomasi, V. Barone, B. Mennucci, M. Cossi, G. Scalmani, N. Rega, G.A. Petersson, H. Nakatsuji, M. Hada, M. Ehara, K. Toyota, R. Fukuda, J. Hasegawa, M. Ishida, T. Nakajima, Y. Honda, O. Kitao, H. Nakai, M. Klene, X. Li, J.E. Knox, H.P. Hratchian, J.B. Cross, C. Adamo, J. Jaramillo, R. Gomperts, R.E. Stratmann, O. Yazyev, A.J. Austin, R. Cammi, C. Pomelli, J.W. Ochterski, P.Y. Ayala, K. Morokuma, G.A. Voth, P. Salvador, J.J. Dannenberg, V.G. Zakrzewski, S. Dapprich, A.D. Daniels, M.C. Strain, O. Farkas, D.K. Malick, A.D. Rabuck, K. Raghavachari, J.B. Foresman, J.V. Ortiz, Q. Cui, A.G. Baboul, S. Clifford, J. Cioslowski, B.B. Stefanov, G. Liu, A. Liashenko, P. Piskorz, I. Komaromi, R.L. Martin, D.J. Fox, T. Keith, M.A. AlLaham, C.Y. Peng, A. Nanayakkara, M. Challacombe, P.M.W. Gill, B. Johnson, W. Chen, M.W. Wong, C. Gonzalez, J.A. Pople, Gaussian 03, Revision C.02, Gaussian, Inc., Wallingford, CT, 2004.
[43] H.B. Schlegel, J. Chem. Phys. 84 (1986) 15.
[44] J. Sponer, P.J. Hobza, J. Phys. Chem. A 104 (2000) 4592.
[45] M.T. Nguyen, S. Creve, L.G. Vanquickenborne, J. Phys. Chem. 100 (1996) 18422.
[46] C. Gonzalez, H.B. Schlegel, J. Phys. Chem. 94 (1990) 5523.
[47] G.D. Purvis, R.J. Bartlett, J. Chem. Phys. 76 (1982) 1910.
[48] (a) R.A. Kendall, T.H. Dunning Jr., J. Chem. Phys. 98 (1992) 6796;
(b) D.E. Woon, T.H. Dunning Jr., J. Chem. Phys. 98 (1992) 1358.
[49] I.S. Ignatyev, Y. Xie, W.D. Allen, H.F. Schaefer, J. Chem. Phys. 107 (1997) 141.
[50] H.B. Schlegel, C. Sosa, Chem. Phys. Lett. 145 (1988) 329.
[51] J.J.W. McDouall, H.B. Schlegel, J. Chem. Phys. 90 (1989) 2363.
[52] L. Farnell, J.A. Pople, L. Radom, J. Phys. Chem. 87 (1983) 79.
[53] J.L. Li, C.Y. Geng, X.R. Huang, C.C. Sun, J. Chem. Theory Comput. 2 (2006) 1551.
[54] A.M. Mebel, E.W.G. Diau, M.C. Lin, K. Morokuma, J. Phys. Chem. 100 (1996) 7517.